

Spin-orbit-parity coupled superconductivity in topological monolayer WTe₂

Ying-Ming Xie,¹ Benjamin T. Zhou,¹ and K. T. Law^{1,*}

¹*Department of Physics, Hong Kong University of Science and Technology, Clear Water Bay, Hong Kong, China*

(Dated: May 30, 2022)

Recent experiments reported gate-induced superconductivity in the monolayer 1T'-WTe₂ which is a two-dimensional topological insulator in its normal state [1, 2]. The in-plane upper critical field B_{c2} is found to exceed the conventional Pauli paramagnetic limit B_p by 1-3 times. The enhancement cannot be explained by conventional spin-orbit coupling which vanishes due to inversion symmetry. In this work, we unveil some distinctive superconducting properties of centrosymmetric 1T'-WTe₂ which arise from the coupling of spin, momentum and band parity degrees of freedom. As a result of this spin-orbit-parity coupling: (i) there is a first-order superconductor-metal transition at B_{c2} much higher than the Pauli paramagnetic limit B_p , (ii) spin-susceptibility is anisotropic with respect to in-plane directions and results in anisotropic B_{c2} and (iii) the B_{c2} exhibits a strong gate dependence as the spin-orbit-parity coupling is significant only near the topological band crossing points. Our theory generally applies to centrosymmetric materials with topological band inversions.

Introduction.— Recently, centrosymmetric monolayer 1T'-structure WTe₂, which is a two-dimensional topological insulator with helical edge states [3–7], has been found to become superconducting upon electro-gating [1, 2]. The coexistence of helical edge states and superconductivity establishes the system as a promising platform to create Majorana fermions [8, 9] and thus attracts wide on-going attention. Interestingly, the in-plane B_{c2} of the superconducting topological insulator was found to be 1-3 times higher than the usual Pauli paramagnetic limit B_p [1, 2].

It has been well established that spin-orbit couplings which lift spin degeneracies in electronic bands can enhance the B_{c2} in noncentrosymmetric superconductors [10, 11]. In particular, a large number of superconducting 2H-structure transition metal dichalcogenides (TMDs) with broken inversion symmetry have been shown to exhibit in-plane B_{c2} several times higher than B_p [12–18]. The enhancement of B_{c2} results from the Ising spin-orbit coupling, which originates from inversion-symmetry-breaking and pins electron spins to out-of-plane directions [12–14]. These superconducting 2H-structure TMDs, such as MoS₂, NbSe₂, WS₂ and TaS₂, are called Ising superconductors [12, 13, 19–23]. Despite similar chemical compositions and layered structures, 1T'-structure WTe₂ respects inversion symmetry and spin-orbit coupling terms which involve only spin and momentum degrees of freedom are forbidden [3–5]. Therefore, the mechanism behind the observed enhancement of B_{c2} remains unknown.

In this work, we show that inversion symmetry, time-reversal symmetry and the topological band inversion (a band inversion involving bands with opposite parities) in 1T'-WTe₂ work together to give rise to spin-orbit-parity coupling (SOPC), with the effect of SOPC on the band structure depicted schematically in Fig.1. The SOPC not only opens a topological gap and creates the helical edge modes [3–7], but also pins the electron spins and renormalizes the effect of external Zeeman fields to

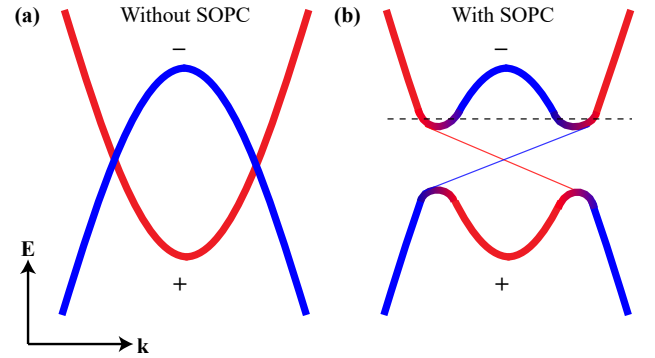


FIG. 1: Schematic band structure of two inverted bands without spin-orbit-parity coupling (SOPC) (a) and with SOPC coupling (b). The +(-) sign labels the even (odd) parity of the band. Bands with even and odd parities in 1T'-WTe₂ originate predominantly from the d - and p - atomic orbitals respectively. In (b), the SOPC opens a topologically nontrivial gap at the band crossing points and edge states emerge (thin lines in the gap). Only states close to the crossing points with heavily mixed orbital parities can experience strong SOPC. The horizontal dashed line in (b) denotes the chemical potential at which superconductivity is observed in the experiment.

enhance the B_{c2} to be much higher than B_p . Importantly, the SOPC dramatically affects the superconducting properties such that: (i) 1T'-WTe₂ undergoes a first-order superconductor-metal transition at B_{c2} , similar to conventional s -wave superconductors [24]. However, the transition happens at a much higher field than B_p ; (ii) the spin susceptibility is anisotropic with respect to in-plane magnetic field directions and results in anisotropic in-plane B_{c2} ; (iii) the B_{c2} is strongly gate-dependent as the SOPC is effective only for states near the topological band crossing points. These properties distinguish superconductors with SOPC from noncentrosymmetric and conventional s -wave superconductors. Comparison among superconductors with SOPC, Ising superconductors and conventional s -wave superconductors is

presented in Table I.

Importantly, SOPC widely exists in topological materials such as superconducting Cu-doped Bi_2Se_3 [25–28]. However, orbital depairing effects in three-dimensional materials overwhelm the Zeeman effect in the superconducting state, which makes the experimental study of SOPC superconductivity a challenging task. Moreover, superconductivity in Cu-doped Bi_2Se_3 sets in when the chemical potential lies high above the band crossing points where the SOPC effect is weak [29, 30]. Therefore, atomically thin $1\text{T}'\text{-WTe}_2$, being superconducting near the band crossing points as depicted in Fig.1b, provides an ideal platform to study spin-orbit-parity coupled superconductivity.

Moreover, an enhanced B_{c2} has been observed in centrosymmetric monolayer $1\text{T}'\text{-MoTe}_2$ [31], which was attributed to Rashba spin-orbit coupling due to gate-induced inversion breaking. Our theory suggests that the B_{c2} enhancement in $1\text{T}'\text{-MoTe}_2$ can be readily explained by the SOPC and the gate-induced inversion breaking is inessential.

Model Hamiltonian of superconducting monolayer $1\text{T}'\text{-WTe}_2$.—The symmetry group of a monolayer $1\text{T}'\text{-WTe}_2$ is generated by time-reversal, one in-plane mirror symmetry, and spatial inversion. These symmetries dictate the form of a four-band Hamiltonian $\mathbf{k} \cdot \mathbf{p}$ which describes the normal state of WTe_2 [3, 32]:

$$H_0(\mathbf{k}) = \epsilon_0(\mathbf{k}) + \mathcal{M}(\mathbf{k})s_z + vk_xs_y + A_xk_xs_x\sigma_y + A_yk_ys_x\sigma_x + A_zk_ys_x\sigma_z, \quad (1)$$

where $\epsilon_0(\mathbf{k}) = t_x^+k_x^2 + t_y^+k_y^2 + \frac{1}{2}t_x'k_y^4 + \frac{1}{2}t_y'k_x^4 - \mu$, $\mathcal{M}(\mathbf{k}) = -\delta + t_x^-k_x^2 + t_y^-k_y^2 - \frac{1}{2}t_x'k_y^4 - \frac{1}{2}t_y'k_x^4$. Here, the s -matrices operate on the orbital degrees of freedom formed by (p, d) -orbitals with opposite parities, and σ -matrices act on the spin space. Notably, δ determines the order of the band at $\mathbf{k} = 0$. When $\delta > 0$, there is a band inversion while the SOPC terms open a topologically non-trivial gap and the system become a topological insulator as schematically depicted in Fig.1b. Derivation of the symmetry allowed terms and the model parameters are given in the Supplementary Materials [32].

In H_0 , the energy dispersions of the bands are given by: $\xi_{\pm}(\mathbf{k}) = \epsilon_0(\mathbf{k}) \pm E(\mathbf{k})$, where $E(\mathbf{k}) = \sqrt{\mathcal{M}^2(\mathbf{k}) + v^2k_x^2 + A^2k^2}$, $Ak = \sqrt{(A_y^2 + A_z^2)k_y^2 + A_x^2k_x^2}$, with each band being two-fold degenerate due to the co-existence of spatial inversion and time-reversal symmetries. The energy bands of H_0 are shown in Fig.2a.

We emphasize that the usual spin-orbit coupling terms which involve \mathbf{k} and σ only are forbidden by inversion symmetry. However, it is possible to have an SOPC term $\hat{\mathbf{g}} \cdot \boldsymbol{\sigma}$, where $\hat{\mathbf{g}} = (A_yk_y, A_xk_x, A_zk_y)s_x$. Importantly, the SOPC term is proportional to s_x and $\langle \Psi(\mathbf{k}) | \hat{\mathbf{g}} \cdot \boldsymbol{\sigma} | \Psi(\mathbf{k}) \rangle$ is significant only for Ψ with strongly hybridized p - and d -orbitals. This happens only near the topological band

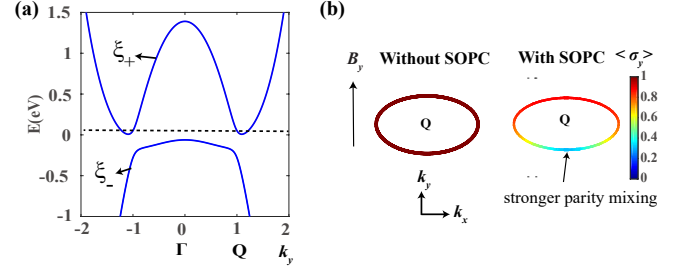


FIG. 2: (a) Normal-state band structure of monolayer WTe_2 . Hybridization between p - and d -bands from SOPC opens a topologically nontrivial gap near $\pm Q$ and results in two Q -valleys in the conduction bands. (b) Expectation value of spin- y component $\langle \sigma_y \rangle$ without (left)/with (right) SOPC on the Fermi surface contours under a weak Zeeman field $\mathbf{B} = B_y \hat{y}$ (Zeeman strength ~ 1 meV, contours around $+Q$ is shown here). The net spin along y -direction induced by B_y is reduced by the pinning due to SOPC.

crossing points as schematically depicted in Fig.1b. Interestingly, superconductivity in $1\text{T}'\text{-WTe}_2$ was observed experimentally when conduction band states near the band crossing points at $\pm Q$ are filled (Fig.2a) with charge density $n \sim 10^{13} \text{cm}^{-2}$ [1, 2]. Thus, $1\text{T}'\text{-WTe}_2$ is an ideal platform to study the effects of SOPC on superconductivity.

Assuming on-site attractive interactions to be dominant, the intra-orbital singlet-pairing phase is expected to be energetically favorable. In this case, the superconducting state under an in-plane magnetic field \mathbf{B} can be described by the Bogoliubovde Gennes Hamiltonian:

$$H_{BdG}(\mathbf{k}) = H_0(\mathbf{k})\eta_3 + \frac{1}{2}g_s u_B \mathbf{B} \cdot \boldsymbol{\sigma} + \Delta\eta_1, \quad (2)$$

where η operates on particle-hole space, u_B is the Bohr magneton, $g_s = 2$ is the Land g factor.

To understand how SOPC affects the magnetic response to an external Zeeman field, it is instructive to project $H_{BdG}(\mathbf{k})$ to a basis formed by the conduction band states with energy $\xi_+(\mathbf{k})$, where superconducting pairing is formed. For convenience, we follow the scheme in Ref.[33–35] to construct a manifestly covariant pseudospin basis (MCPB) $\{|\mathbf{k}, \alpha\rangle, |\mathbf{k}, \beta\rangle\}$ for the conduction band $\xi_+(\mathbf{k}) \equiv \xi_{\mathbf{k}}$ (more details see Supplementary Materials [32]), which has a simple transformation rule under any point group symmetry \mathcal{G} : $\mathcal{G}|\mathbf{k}, \alpha\rangle = U_{\alpha\beta}(\mathcal{G})|\mathcal{G}\mathbf{k}, \beta\rangle$, and $|\mathbf{k}, \alpha\rangle, |-\mathbf{k}, \beta\rangle$ are related by time reversal symmetry: $\mathcal{T}|\mathbf{k}, \alpha\rangle = (i\sigma_y)_{\alpha\beta} |-\mathbf{k}, \beta\rangle$. Here, $U_{\alpha\beta}(\mathcal{G})$ is the $\text{SU}(2)$ representation of \mathcal{G} . By projecting $H_{BdG}(\mathbf{k})$ into the subspace $(\psi_{\mathbf{k}, \alpha}^\dagger, \psi_{\mathbf{k}, \beta}^\dagger, \psi_{-\mathbf{k}, \beta}, -\psi_{-\mathbf{k}, \alpha})$, the effective pairing Hamiltonian has the form:

$$H_{\text{eff}}(\mathbf{k}) = \xi_{\mathbf{k}}\eta_3 + \frac{1}{2}g_s u_B \mathbf{B} \cdot \tilde{\boldsymbol{\sigma}}(\mathbf{k}) + \Delta\eta_1, \quad (3)$$

where $\tilde{\sigma}_i^{l,l'}(\mathbf{k}) = \langle \mathbf{k}, l | \sigma_i | \mathbf{k}, l' \rangle = \sum_j a_{ij}(\mathbf{k}) \rho_j^{l,l'}$ (ρ_j : Pauli matrix in the pseudospin basis) is the projected spin

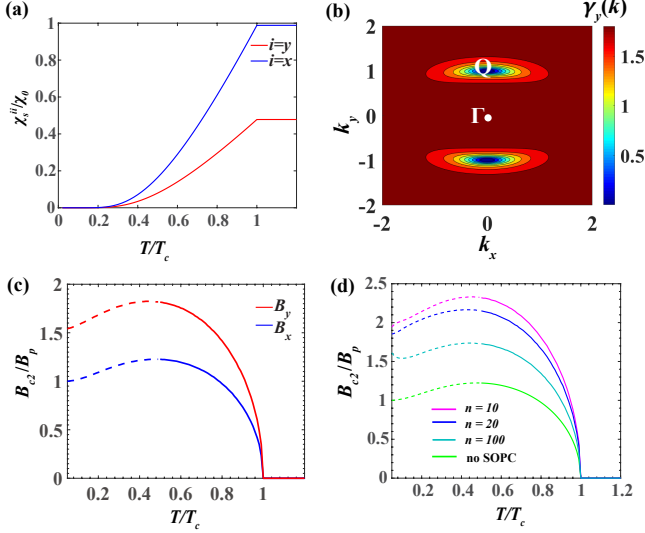


FIG. 3: Enhancement of B_{c2} via SOPC for 1T'-WTe₂. (a) Spin susceptibility χ_n^{ii} ($i = x, y$) as a function of temperature T , where the SOPC strength is $A_y = 0.855$ eV·Å, Fermi energy $E_F = 100$ meV. We set $T_c = 1$ K according to experimental observations. (b) Value of γ_y at different \mathbf{k} . $\gamma_y(\mathbf{k})$ approaches zero near the band minimum at $\pm Q$. (c) $B_{c2} - T_c$ curves for $\mathbf{B} = B_x \hat{x}$ (blue) and $\mathbf{B} = B_y \hat{y}$ (red). Other parameters are the same as in (a). (d) $B_{c2} - T_c$ curves for $\mathbf{B} = B_y \hat{y}$ with different carrier density n in units of 10^{12} cm⁻² and $A_y = 1.71$ eV·Å. The case without SOPC (light green curve) is presented for reference.

operator in the pseudospin subspace, and the effect of SOPC on electron spins are encoded in the coefficients $a_{ij}(\mathbf{k})$. It is clear from Eq.3 that the Zeeman effect due to external magnetic fields is renormalized by the SOPC term. The explicit forms of $a_{ij}(\mathbf{k})$ are given in Section II of the Supplementary Material [32]. To be specific, consider the $A_y k_y$ term only and with an applied magnetic field along the y -direction, we have $B_y \tilde{\sigma}_y = B_y \sqrt{1 - A_y^2 k_y^2 / E^2(\mathbf{k})} \rho_y$. Therefore, the Zeeman effect is reduced by the SOPC term.

To demonstrate the spin-pinning effect encoded in $a_{ij}(\mathbf{k})$, we assume a weak Zeeman field $\mathbf{B} = B_y \hat{y}$ in H_{eff} and plot the Zeeman field induced spin expectation value in the y -direction $\langle \sigma_y \rangle$ for states near the Q -point with and without SOPC in Fig.2b. Evidently, without SOPC, spins along the Fermi surface contours can freely align with B_y . In contrast, in the presence of SOPC, spins at different \mathbf{k} are pinned predominantly to the x -direction as the $A_y k_y s_x \sigma_x$ term dominates [32]. It is important to note that in Fig.2b, the spin pinning is much stronger for states with smaller k_y near the band crossing point due to the stronger mixing between p - and d -orbitals in these states. This clearly demonstrates the SOPC effect is not determined by the spin-orbit coupling part $A_y k_y \sigma_x$ alone, but also largely governed by the parity mixing operator s_x . In the next section, we show that the spin pinning by

SOPC terms, which reduces the normal-state spin susceptibility, provides the origin behind the enhancement of B_{c2} in centrosymmetric superconductors with SOPC.

Enhancement, anisotropy and gate dependence of in-plane B_{c2} . —Phenomenologically, the normal-state and superconducting free energy densities due to an external in-plane field \mathbf{B} ($B = |\mathbf{B}|$) and pairing can be written as $f_n(B) = -\frac{1}{2} \chi_n B^2$, and $f_s(B) = f_{\text{cond}} + f_{\text{spin}}$ respectively. Here, χ_n / χ_s is the normal-state/superconducting spin susceptibility, $f_{\text{cond}} = -\frac{1}{2} N(E_F) \Delta_0^2$, with $\Delta_0 = \Delta(B = 0)$, is the zero-field condensation energy with $N(E_F)$ being the density of states at Fermi energy, and $f_{\text{spin}} = -\frac{1}{2} \chi_s B^2$ is the spin magnetic energy in the superconducting state. B_{c2} can be estimated by identifying the point $f_n(B) = f_s(B)$, yielding $B_{c2} \approx B_p \sqrt{\chi_0 / (\chi_n - \chi_s)}$, where $B_p = \Delta_0 / (\sqrt{2} \mu_B)$, and $\chi_0 = 2N(E_F) u_B^2$ is the Pauli spin susceptibility of free electron gas. Clearly, B_{c2} can be enhanced to be higher than B_p via: (i) a reduced normal-state susceptibility $\chi_n < \chi_0$, and (ii) a residue superconducting spin susceptibility $\chi_s \neq 0$. As shown in the MCPB basis, H_{eff} has the form of a spin-singlet superconductor, we expect that the superconducting ground state cannot respond to a weak external Zeeman fields, which implies $\chi_s = 0$ in the $T \rightarrow 0$ limit.

To demonstrate the vanishing χ_s in WTe₂, we calculate the superconducting spin susceptibility χ_s^{ii} ($i = x, y$) given by [36, 37]:

$$\chi_s^{ij} = -\frac{1}{2} u_B^2 k_B T \sum_{\mathbf{k}, \omega_n} \text{Tr}[\tilde{\sigma}_i \mathcal{G}(\mathbf{k}, i\omega_n) \tilde{\sigma}_j \mathcal{G}(\mathbf{k}, i\omega_n)], \quad (4)$$

where $\mathcal{G}(\mathbf{k}, i\omega_n) = (i\omega_n - \xi_{\mathbf{k}} \eta_3 - \Delta \eta_1)^{-1}$ is the Gor'kov Green's function obtained from $H_{\text{eff}}(\mathbf{k})$ in Eq.3 under zero magnetic field. T is the temperature, and $\omega_n = (2n + 1)\pi / k_B T$ denotes the fermionic Matsubara frequency. By taking the Matsubara sum, the in-plane χ_s^{ii} ($i = x, y$) can be written as:

$$\chi_s^{ii} = \frac{1}{2} u_B^2 \beta \sum_{\mathbf{k}} \gamma_i(\mathbf{k}) \frac{1}{1 + \cosh(\beta \sqrt{\xi_{\mathbf{k}}^2 + \Delta^2})}. \quad (5)$$

Here $\beta = 1/k_B T$, and $\gamma_i(\mathbf{k}) = 2 \sum_j a_{ij}^2(\mathbf{k})$ characterizes the renormalization effect on spins due to SOPC. Clearly, the denominator in the summand in Eq. (5) diverges as $T \rightarrow 0$ due to a finite superconducting gap Δ , thus $\chi_s^{ii}(T \rightarrow 0) = 0$ (Fig.3a).

The vanishing χ_s^{ii} leaves us with the mechanism of enhanced B_{c2} via reduced χ_n . Note that χ_n is directly given by $\chi_s(\Delta = 0)$ in Eq. (5), *i.e.*,

$$\chi_n^{ii} = \frac{1}{2} u_B^2 \beta \sum_{\mathbf{k}} \gamma_i(\mathbf{k}) \frac{1}{1 + \cosh(\beta \xi_{\mathbf{k}})} = u_B^2 N(E_F) \gamma_i(E_F), \quad (6)$$

where $\gamma_i(E_F) = \int d^2 \mathbf{k} \gamma_i(\mathbf{k}) \delta(\xi_{\mathbf{k}} - E_F) / \int d^2 \mathbf{k} \delta(\xi_{\mathbf{k}} - E_F)$ is the averaged renormalization factor due to SOPC over the Fermi surface (see Supplementary Material Sec. III [32]).

As shown in Eq.6, the normal-state spin susceptibility of a superconductor with SOPC is given by $\chi_n^{ii} = \gamma_i(E_F)\chi_0/2$, with a renormalization factor $\gamma_i(E_F)/2$ due to SOPC. In the low temperature limit, the in-plane critical field along i -direction ($i = x, y$) is directly related to the Pauli limit by $B_{c2}^{ii} = B_p\sqrt{\chi_0/\chi_n^{ii}} = B_p\sqrt{2/\gamma_i(E_F)}$, which implies $B_{c2} > B_p$ when $\gamma_i(E_F) < 2$.

To show the reduced χ_n^{yy} , we plot the momentum-space profile of $\gamma_y(\mathbf{k})$ in the conduction band (Fig.3b). Evidently, $\gamma_y(\mathbf{k}) < 2$ holds throughout the whole Brillouin zone. As a result, $\gamma_y(E_F) < 2$ in general, leading to $\chi_n^{yy} < \chi_0$ as consistent with the result in Fig.3a (red curve) where $\chi_s^{yy} = \chi_n^{yy} < \chi_0$ for $T > T_c$.

In contrast, we noticed that $\chi_s^{xx} = \chi_n^{xx} \approx \chi_0$ for $T > T_c$ (blue curve in Fig.3a). This is due to the fact that $\mathbf{B} = B_x\hat{x}$, being collinear with the dominant SOPC term $A_y k_y s_x \sigma_x$, can freely align spins to the x -direction. As a result, $B_{c2}^{yy} > B_p$ while $B_{c2}^{xx} \approx B_p$ as shown in the $B_{c2}-T_c$ curves in Fig.3c obtained by solving the linearized gap equation:

$$\frac{2}{U/V} = k_B T \sum_{\mathbf{k}} \sum_n \text{Tr}[G^{(0)}(\mathbf{k}, i\omega_n) \rho_y G^{(0)T}(-\mathbf{k}, -i\omega_n) \rho_y]. \quad (7)$$

Here, U is electron-phonon interaction strength, V is the sample volume, $G^{(0)}(\mathbf{k}, i\omega_n)$ is the normal state Green's function of $H_{\text{eff}}(\mathbf{k})$ given in Eq. 3 (see Sec. IV of Supplementary Materials [32] for details). Thus, the B_{c2} of the SOPC superconductor exhibits a strong anisotropy due to the anisotropy in SOPC. This special property of SOPC superconductor is very different from the isotropic B_{c2} and χ_s in both Ising superconductors and conventional superconductors as summarized in Table I.

Interestingly, the momentum-space profile of the SOPC-induced renormalization factor $\gamma_y(\mathbf{k})$ (Fig.3b) has a strong \mathbf{k} -dependence. In particular, the renormalization is strongest (signified by a strongly reduced value of $\gamma_y(\mathbf{k})$) near the band crossing points at $\pm Q$. As E_F increases upon gating, outer Fermi circles enclosing $\pm Q$ are accessed and the value of $\gamma_y(\mathbf{k})$ approaches the value of $\gamma_0 = 2$ for free electron gas. This again reflects the *parity-mixing* nature of SOPC: the spin pinning effect due to SOPC terms is strongest near the band crossing points at $\pm Q$ where the p - and d -orbitals are strongly mixed. As \mathbf{k} deviates from $\pm Q$, the parity mixing becomes weaker and the spin pinning effect is suppressed.

Such strong dependence of $\gamma_y(\mathbf{k})$ on Fermi level implies a strong gate-dependence in B_{c2}^{yy} . This is explicitly demonstrated by solving the linearized gap equation at different values of carrier density n (Fig.3d). Consistent with our discussions above, as n increases, the enhancement of B_{c2} is reduced.

It is worth noting that for the SOPC superconductor WTe₂, the low temperature sectors of the $B_{c2}-T_c$ curves obtained by linearized gap equations (dashed segments in the range $0 < T < T_1 \approx 0.5T_c$) do not represent the

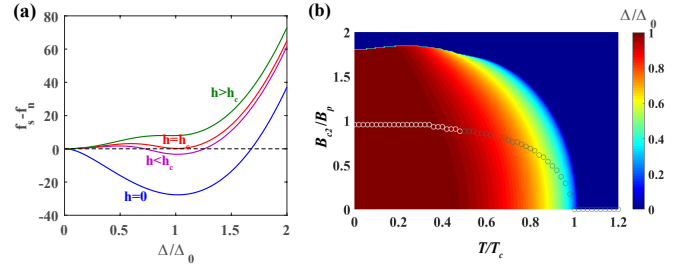


FIG. 4: (a) Landscapes of $f_s - f_n$ at $T = 0.1T_c$ in units of meV under $B = 0, 1.8B_p, 1.93B_p, 2.2B_p$. $B_{c2} \sim 1.93B_p$, with $\Delta_0 \approx 1.764k_B T_c$ at $B, T = 0$. (b) $B - T$ phase diagram from minimizing $f_s - f_n$ with $A_y = 1.71 \text{ eV} \cdot \text{\AA}$ and $n = 10 \times 10^{12} \text{ cm}^{-2}$. The color represents the magnitude of Δ at different B and T . The line of circles represent the values of B_{c2} in a conventional superconductor, where $B_{c2}(T = 0) = B_p$. A first-order transition also occurs in the low temperature regime [24] (indicated by white circles).

true values of B_{c2} but the supercooling critical field instead [24]. As we discuss next, the superconductor-metal transition at B_{c2} in this regime is in fact first-order in nature, which invalidates the assumption $\lim_{B \rightarrow B_{c2}} \Delta \rightarrow 0$ for the scheme of linearizing the gap function at phase boundaries.

First-order phase transition at B_{c2} in low temperature regime.—To understand the nature of the phase transition at B_{c2} in the low temperature regime, we study how the free energy of a superconducting monolayer WTe₂ evolves under \mathbf{B} . Based on the full $H_{BdG}(\mathbf{k})$ in Eq.2, the free energy of the SOPC superconductor as a function of Δ can be obtained as [32, 38]:

$$f_s = \frac{V|\Delta|^2}{U} - \frac{1}{\beta} \sum_{\mathbf{k}, n} \ln(1 + e^{-\beta \epsilon_{\mathbf{k}, n}}), \quad (8)$$

where $\epsilon_{\mathbf{k}, n}$ are the quasi-particle energies of $H_{BdG}(\mathbf{k})$. With fixed SOPC strength $A_y = 1.71 \text{ eV} \cdot \text{\AA}$ and carrier density $n = 10 \times 10^{12} \text{ cm}^{-2}$, the evolution of $f_s - f_n$ at $T = 0.1T_c$ under increasing B is shown in Fig.4a (note that $f_n \equiv f_s(\Delta = 0)$). Clearly, for $0 < B < B_{c2}$, a local minimum in the free energy landscape develops at $\Delta = 0$ (purple curve) and eventually becomes the global minimum at $B = B_{c2}$ (red curve), where the superconductor-metal transition occurs. Notably, Δ drops abruptly to zero at B_c , which signifies a first-order phase transition.

The full self-consistent $B - T$ phase diagram from minimizing $f_s - f_n$ is shown in Fig.4b with the phase boundary at B_{c2} accurately captured for all $T < T_c$. In accord with Fig.4a, the order parameter drops abruptly to zero at B_{c2} in the low temperature regime. We note that the mechanism of first-order transition in the low temperature limit for superconductors with SOPC is similar to a conventional superconductor, but the phase transition happens much higher than B_p in SOPC superconductors as illustrated in Fig.4b. In particular, this distinc-

TABLE I: Comparison among centrosymmetric spin-orbit-parity-coupled(SOPC), Ising and conventional superconductivity.

Type of superconductors	SOPC	Ising	Conventional
Pairing correlations	Singlet	Singlet-triplet mixing	Singlet
$\chi_s(T=0)$	Zero	Finite	Zero
In-plane B_{c2}	$> B_p$	$> B_p$	$= B_p$
B -driven superconductor-metal transition as $T \rightarrow 0$	First-order	Continuous	First-order
Directional dependence of in-plane B_{c2}/χ_s	Anisotropic	Isotropic	Isotropic

tive first-order transition in the SOPC superconductor WTe₂ is very different from the continuous phase transition found in noncentrosymmetric Ising superconductors such as NbSe₂ due to a significant χ_s induced by Ising spin-orbit couplings [18, 39, 40].

Conclusion and Discussions.— In this work, we identified a new class of centrosymmetric spin-orbit-parity coupled superconductors where SOPC leads to enhancement of in-plane B_{c2} higher than B_p . In particular, we explained how the strong parity-mixing due to SOPC near the topologically nontrivial gap edge gives rise to a strongly enhanced B_{c2} in the superconducting topological monolayer WTe₂ with low electron carrier density. We further pointed out that the B_{c2} of SOPC superconductors generally shows an anisotropy in in-plane field directions. These properties uncovered in this work are distinguished from both conventional superconductors and Ising superconductors as summarized in Table I.

While we considered the case of a clean SOPC superconductor in the main text, we briefly discuss here the effect of disorder on the enhancement of B_{c2} . By including potential fluctuation scattering and spin-orbit scattering effects in the Green function and the vertex correction to the spin susceptibility in disordered samples, we show that the B_{c2} is not sensitive to potential fluctuation scattering but a finite χ_s is induced by spin-orbit scattering in the superconducting state, which further enhances the B_{c2} [32]. This explains why a higher B_{c2} was observed in the more disordered sample in Ref.[1] where $B_{c2} \approx 4B_p$.

Note.—After presenting the main findings of this work [41], we noticed that the enhancement of B_{c2} was observed in non-topological centrosymmetric materials without band inversion such as in few-layer stanene and ultrathin PdTe₂ [42–44]. The enhanced B_{c2} in these materials originates mainly from \mathbf{k} -independent atomic spin-orbital coupling, which is very different from the SOPC effect studied in our work.

Acknowledgments.—The authors are thankful for illuminating discussions with Wenyu He, Noah F.Q. Yuan and particularly for Mengli Hu and Junwei Liu for showing us the band structure of 1T'-WTe₂ from first-principle calculations. KTL acknowledges the support of the Croucher Foundation, Dr. Tai-chin Lo Foundation and HKRGC through C6025-19G, C6026-16W, 16310219 and 16309718.

* Corresponding author.

phlaw@ust.hk

- [1] V. Fatemi, S. Wu, Y. Cao, L. Bretheau, Q. D. Gibson, K. Watanabe, T. Taniguchi, R. J. Cava and P. Jarillo-Herrero, *Science* **362**, 926–929 (2018).
- [2] E. Sajadi, T. Palomaki, Z. Fei, W. Zhao, P. Bement, C. Olsen, S. Luescher, X. Xu, J. A. Folk and D. H. Cobden, *Science* **362**, 922–925 (2018).
- [3] X. Qian, J. Liu, L. Fu, and J. Li, *Science* **346**, 1344 (2014).
- [4] L. Muechler, A. Alexandradinata, T. Neupert, and R. Car, *Phys. Rev. X* **6**, 041069 (2016).
- [5] S. Tang et al., *Nat. Phys.* **13**, 683 (2017).
- [6] Z. Fei, T. Palomaki, S. Wu, W. Zhao, X. Cai, B. Sun, P. Nguyen, J. Finney, X. Xu and D. H. Cobden, *Nat. Phys.* **13**, 677 (2017).
- [7] S. Wu, V. Fatemi, Q. D. Gibson, K. Watanabe, T. Taniguchi, R. J. Cava, and P. Jarillo-Herrero, *Science* **359**, 76 (2018).
- [8] L. Fu and C. L. Kane, *Phys. Rev. B* **79**, 161408 (2009).
- [9] J. Nilsson, A. R. Akhmerov, and C. W. J. Beenakker, *Phys. Rev. Lett.* **101**, 120403 (2008).
- [10] P. A. Frigeri, D. F. Agterberg, A. Koga and M. Sigrist, *Phys. Rev. Lett.* **92**, 097001 (2004).
- [11] Gor'kov, Lev P. and Rashba, Emmanuel I., *Phys. Rev. Lett.* **87**, 037004 (2001).
- [12] Lu, J. M., Zheliuk, O., Leermakers, I., Yuan, N. F. Q., Zeitler, U., Law, K. T., Ye, J. T., *Science* **350**, 1353–1357 (2015).
- [13] X. Xi, Z. Wang, W. Zhao, J.-H. Park, K. T. Law, H. Berger, L. Forr, J. Shan, and K. F. Mak, *Nat. Phys.* **12**, 139 (2016).
- [14] Y. Saito et al., *Nature Physics* **12**, 144149 (2016).
- [15] S. C. de la Barrera, M. R. Sinko, D. P. Gopalan, N. Sivadas, K. L. Seyler, K. Watanabe, T. Taniguchi, A. W. Tsen, X. Xu, D. Xiao, and B. M. Hunt, *Nature Communications* **9**, 1427 (2018).
- [16] J. Lu, O. Zheliuk, Q. Chen, I. Leermakers, N. E. Hussey, U. Zeitler, and J. Ye, *Proc. Natl. Acad. Sci. U.S.A.* **115**, 3551 (2018).
- [17] Y. Xing, K. Zhao, P. Shan, F. Zheng, Y. Zhang, H. Fu, Y. Liu, M. Tian, C. Xi, H. Liu, J. Feng, X. Lin, S. Ji, X. Chen, Q.-K. Xue, and J. Wang, *Nano Lett.* **17**, 6802 (2017).
- [18] E. Sohn, X. Xi, W.-Y. He, S. Jiang, Z. Wang, K. Kang, J.-H. Park, H. Berger, L. Forró, K. T. Law, J. Shan, and K. F. Mak, *Nature Materials* **17**, 504 (2018).
- [19] B. T. Zhou, N. F. Q. Yuan, H.-L. Jiang, K. T. Law, *Phys. Rev. B* **93**, 180501 (2016).

- [20] W.-Y. He, B. T. Zhou, J. J. He, N. F. Q. Yuan, T. Zhang, K. T. Law, *Communications Physics* **1**, 40 (2018).
- [21] G. Sharma and S. Tewari, *Phys. Rev. B* **94**, 094515 (2016).
- [22] S. Ilić, J. S. Meyer, and M. Houzet, *Phys. Rev. Lett.* **119**, 117001 (2017).
- [23] J. Zhang and V. Aji, *Phys. Rev. B* **94**, 060501(R) (2016).
- [24] K. Maki and T. Tsuneto, *Progress of Theoretical Physics* **31**, 945 (1964).
- [25] H. Zhang, C.-X. Liu, X.-L. Qi, X. Dai, Z. Fang, and S.-C. Zhang, *Nat. Phys.* **5**, 438 (2009).
- [26] C.-X. Liu, X.-L. Qi, H. Zhang, X. Dai, Z. Fang, and S.-C. Zhang, *Phys. Rev. B* **82**, 045122 (2010).
- [27] L. Fu and E. Berg, *Phys. Rev. Lett.* **105**, 097001 (2010).
- [28] T. Hashimoto, K. Yada, A. Yamakage, M. Sato, and Y. Tanaka, *Journal of the Physical Society of Japan* **82**, 044704 (2013).
- [29] Y. S. Hor, A. J. Williams, J. G. Checkelsky, P. Roushan, J. Seo, Q. Xu, H. W. Zandbergen, A. Yazdani, N. P. Ong, and R. J. Cava, *Phys. Rev. Lett.* **104**, 057001 (2010).
- [30] L. A. Wray, S.-Y. Xu, Y. Xia, Y. S. Hor, D. Qian, A. V. Fedorov, H. Lin, A. Bansil, R. J. Cava, and M. Z. Hasan, *Nat. Phys.* **6**, 855 (2010).
- [31] D. Rhodes, N. F. Yuan, Y. Jung, A. Antony, H. Wang, B. Kim, Y.-c. Chiu, T. Taniguchi, K. Watanabe, K. Barmak, L. Balicas, C. R. Dean, X. Qian, L. Fu, A. N. Pasupathy, and J. Hone, arXiv:1905.06508 (2019).
- [32] See Supplemental Material for (1) $k \cdot p$ model of monolayer $1T'$ -WTe₂; (2) effective pairing Hamiltonian for SOPC superconductors; (3) Pauli spin susceptibility and renormalization factor γ_i ; (4) B_{c2} from the linearized gap equation; (5) derivation of superconducting free energy; (6) spin susceptibility with non-magnetic impurity scattering.
- [33] S.-K. Yip, *Phys. Rev. B* **87**, 104505 (2013).
- [34] L. Fu, *Phys. Rev. Lett.* **115**, 026401 (2015).
- [35] J. W. F. Venderbos, V. Kozii, and L. Fu, *Phys. Rev. B* **94**, 180504 (2016).
- [36] P. A. Frigeri, D. F. Agterberg, and M. Sigrist, *New Journal of Physics* **6**, 115 (2004).
- [37] A. Abrikosov and L. Gorkov, *Sov. Phys. JETP* **15**, 752 (1962).
- [38] A. Altland and B. D. Simons, *Condensed matter field theory* (Cambridge University Press, 2010).
- [39] R. Wakatsuki and K. T. Law, arXiv:1604.04898 (2016).
- [40] Y. Xie, B. T. Zhou, T. K. Ng, and K. T. Law, *Phys. Rev. Research* **2**, 013026 (2020).
- [41] Y. Xie, W. He, and K. T. Law, in APS Meeting Abstracts (2019). <https://meetings.aps.org/Meeting/MAR19/Session/P09.5>.
- [42] C. Wang, B. Lian, X. Guo, J. Mao, Z. Zhang, D. Zhang, B.-L. Gu, Y. Xu, and W. Duan, *Phys. Rev. Lett.* **123**, 126402 (2019).
- [43] J. Falson, Y. Xu, M. Liao, Y. Zang, K. Zhu, C. Wang, Z. Zhang, H. Liu, W. Duan, K. He, H. Liu, J. H. Smet, D. Zhang, and Q.-K. Xue, *Science* **367**, 1454 (2020).
- [44] Y. Liu, Y. Xu, J. Sun, C. Liu, Y. Liu, C. Wang, Z. Zhang, K. Gu, Y. Tang, C. Ding, H. Liu, H. Yao, X. Lin, L. Wang, Q. Xue, and J. Wang, arXiv:1904.12719 (2019).

Supplementary Material for ‘Spin-orbit-parity coupled superconductivity in topological monolayer WTe₂’

Ying-Ming Xie,¹ Benjamin T. Zhou,¹ and K. T. Law^{1,*}

¹*Department of Physics, Hong Kong University of Science and Technology, Clear Water Bay, Hong Kong, China*
(Dated: May 30, 2022)

$\mathbf{k} \cdot \mathbf{p}$ MODEL OF MONOLAYER 1T'-WTe₂

Here, we present detailed derivation of the $\mathbf{k} \cdot \mathbf{p}$ Hamiltonian in Eq.1 of the main text based on the mirror symmetry M_y , inversion symmetry P and time reversal symmetry T . According to first principle calculations [S1–S6], the dominant orbitals near Γ point transforms as p_y and d_{yz} orbitals, which have opposite spatial parities and are odd under M_y . In the basis $(|p_y, \uparrow\rangle, |p_y, \downarrow\rangle, |d_{yz}, \uparrow\rangle, |d_{yz}, \downarrow\rangle)$, the symmetry operators are given by: $M_y = -i\sigma_y$, $P = s_z$, $T = i\sigma_y K$. Using the method of invariant [S7], we write down a four-band $\mathbf{k} \cdot \mathbf{p}$ model as

$$H_0(\mathbf{k}) = \begin{pmatrix} \epsilon_p(\mathbf{k}) & 0 & -ivk_x + A_zk_y & -iA_xk_x + A_yk_y \\ 0 & \epsilon_p(\mathbf{p}) & iA_xk_x + A_yk_y & -ivk_x - A_zk_y \\ ivk_x + A_zk_y & -iA_xk_x + A_yk_y & \epsilon_d(\mathbf{k}) & 0 \\ iA_xk_x + A_yk_y & ivk_x - A_zk_y & 0 & \epsilon_d(\mathbf{k}) \end{pmatrix}, \quad (\text{S1})$$

where $\epsilon_p(\mathbf{k}) = -t_{xp}k_x^2 - t_{yp}k_y^2 - \mu_p$, $\epsilon_d(\mathbf{k}) = -t_{xd}k_x^2 - t_{yd}k_y^2 + t'_xk_x^4 + t'_yk_y^4 - \mu_d$. The effective parameters in Eq.S1 (listed in Table S1) are determined by fitting the *ab initio* band structure[S1, S2]. Note that $A_x, A_z < A_y$ due to the highly anisotropic crystal symmetry of 1T'-WTe₂ and the values of A_x, A_y, A_z in Table S1 are mainly as a reference for the scale, which is sensitive to the gap and hard to be solely determined by the *ab initio* calculation.

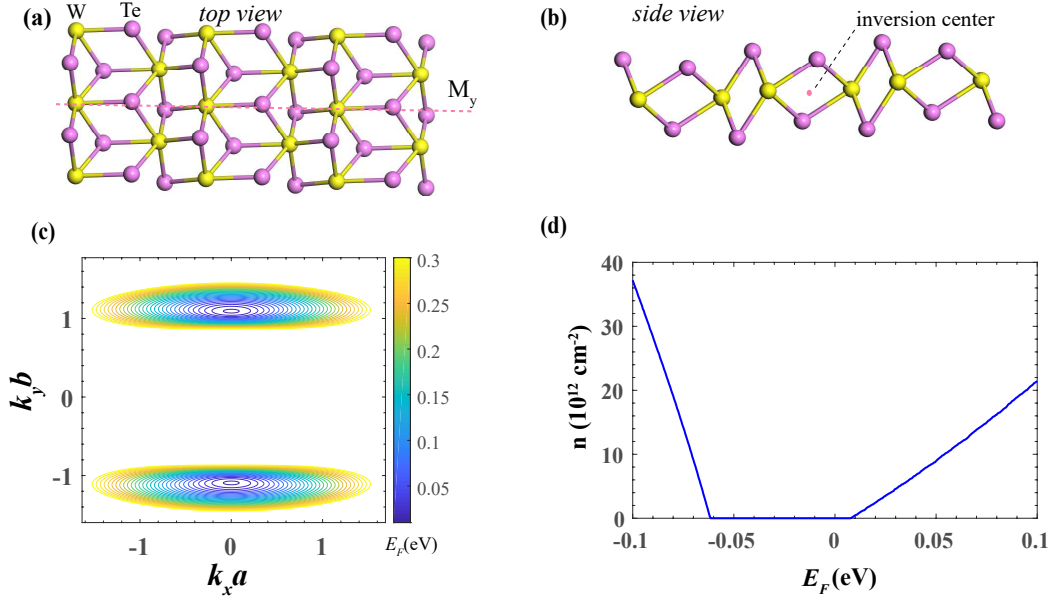


FIG. S1: Crystal structure and band structure of monolayer 1T'-WTe₂. (a) Top view and (b) side view of monolayer WTe₂. W/Te atoms are depicted in yellow/purple. M_y axis and inversion center are highlighted in pink dashed line and pink dot, respectively. (c) Fermi circles for Fermi energy E_F in the range $0 \sim 0.3$ eV from the model Hamiltonian (S1). The separation between adjacent Fermi circles is 0.01 eV. The corresponding parameters are listed in Table S1. (d) Carrier density $n = \langle \psi^\dagger(\mathbf{r})\psi(\mathbf{r}) \rangle$ versus E_F .

TABLE S1: Parameters of $\mathbf{k} \cdot \mathbf{p}$ Hamiltonian (S1). The lattice constants are $a = 6.31\text{\AA}$, $b = 3.49\text{\AA}$.

$\mu_p(\text{eV})$	$\mu_d(\text{eV})$	$t_{xp}(\text{eV} \cdot \text{\AA}^2)$	$t_{yp}(\text{eV} \cdot \text{\AA}^2)$	$t_{xd}(\text{eV} \cdot \text{\AA}^2)$	$t_{yd}(\text{eV} \cdot \text{\AA}^2)$	$t'_x(\text{eV} \cdot \text{\AA}^4)$	$t'_y(\text{eV} \cdot \text{\AA}^4)$	$v(\text{eV} \cdot \text{\AA})$	$A_x(\text{eV} \cdot \text{\AA})$	$A_y(\text{eV} \cdot \text{\AA})$	$A_z(\text{eV} \cdot \text{\AA})$
-1.39	0.062	12.45	18.48	-2.58	2.68	-7.79	26.65	2.34	0.17	0.57	0.07

EFFECTIVE PAIRING HAMILTONIAN FOR SOPC SUPERCONDUCTORS

The normal state electronic property is captured by the $\mathbf{k} \cdot \mathbf{p}$ model (Eq.S1). To further describe the superconducting topological monolayer WTe_2 , we first write down the Bogoliubovde Gennes Hamiltonian

$$H_{BdG}(\mathbf{k}) = H_0(\mathbf{k})\eta_3 + \frac{1}{2}gu_B\mathbf{B} \cdot \boldsymbol{\sigma} + \Delta\eta_1, \quad (\text{S2})$$

(same as Eq.2 of the main text). Here η_i is the Pauli matrix defined in the particle-hole basis. With the full $H_{BdG}(\mathbf{k})$, the spin susceptibility and free energy of the system can be readily calculated numerically. However, since superconducting pairing forms from states near Fermi energy only, we can further obtain an effective pairing Hamiltonian by projecting $H_0(\mathbf{k})$ to the conduction bands where the gate-induced superconductivity occurs. As mentioned in the main text, a convenient choice is the manifestly covariant pseudospin basis. In the following, we first derive the corresponding pseudospin basis $|\mathbf{k}, \alpha\rangle, |\mathbf{k}, \beta\rangle$ of the doubly degenerate conduction band. Then, we project the Hamiltonian $H_{BdG}(\mathbf{k})$ into the subspace $\{\psi_{\mathbf{k},\alpha}^\dagger, \psi_{\mathbf{k},\beta}^\dagger, \psi_{-\mathbf{k},\beta}, -\psi_{-\mathbf{k},\alpha}\}$, where $\psi_{\mathbf{k},\alpha}^\dagger, \psi_{\mathbf{k},\beta}^\dagger$ is the creation operator of $|\mathbf{k}, \alpha\rangle, |\mathbf{k}, \beta\rangle$.

Note that the Hamiltonian (S1) can be rewritten as

$$H_0(\mathbf{k}) = \epsilon_0(\mathbf{k}) + \mathcal{M}(\mathbf{k})s_z + vk_xs_y + A_xk_xs_x\sigma_y + A_yk_ys_x\sigma_x + A_zk_ys_x\sigma_z, \quad (\text{S3})$$

where

$$\epsilon_0(\mathbf{k}) = t_x^+k_x^2 + t_y^+k_y^2 + \frac{1}{2}t'_xk_y^4 + \frac{1}{2}t'_yk_y^4 - \mu_0, \quad (\text{S4})$$

$$\mathcal{M}(\mathbf{k}) = -\delta + t_x^-k_x^2 + t_y^-k_y^2 - \frac{1}{2}t'_xk_x^4 - \frac{1}{2}t'_yk_y^4. \quad (\text{S5})$$

Here $t_x^\pm = -(t_{xp} \pm t_{xd})/2$, $t_y^\pm = -(t_{yp} \pm t_{yd})/2$, $\mu_0 = (\mu_d + \mu_p)/2$, $\delta = (\mu_p - \mu_d)/2$. The spin-orbit-parity coupling(SOPC) terms are given by the $A_i(i = x, y, z)$ -terms involving the spin σ -matrices. Due to the presence of SOPC terms, we first diagonalize the spin part with the basis $|+1\rangle = \cos \frac{\theta_{\mathbf{k}}}{2} |\uparrow\rangle + \sin \frac{\theta_{\mathbf{k}}}{2} e^{i\phi_{\mathbf{k}}} |\downarrow\rangle$, $|-1\rangle = -\sin \frac{\theta_{\mathbf{k}}}{2} e^{-i\phi_{\mathbf{k}}} |\uparrow\rangle + \cos \frac{\theta_{\mathbf{k}}}{2} |\downarrow\rangle$. Here $\theta_{\mathbf{k}}$ and $\phi_{\mathbf{k}}$ are defined by $(A_yk_y, A_xk_x, A_zk_y) = Ak(\sin \theta_{\mathbf{k}} \cos \phi_{\mathbf{k}}, \sin \theta_{\mathbf{k}} \sin \phi_{\mathbf{k}}, \cos \theta_{\mathbf{k}})$. Then

$$H_0(\mathbf{k}) = \epsilon_0(\mathbf{k}) + \mathcal{M}(\mathbf{k})s_z + vk_xs_y + Ak_s_x\tau_z. \quad (\text{S6})$$

τ_z is the Pauli matrix defined in $(|+1\rangle, |-1\rangle)$ space. By straightforward diagonalization, the eigenenergy can be obtained as $\epsilon_\pm(\mathbf{k}) = \epsilon_0(\mathbf{k}) \pm \sqrt{\mathcal{M}^2(\mathbf{k}) + v^2k_x^2 + A^2k^2}$, and each band has a two-fold degeneracy due to time-reversal and spatial inversion. The corresponding eigenvectors of the conduction band with $\epsilon_+(\mathbf{k})$ are given by

$$|\mathbf{k}, \alpha'\rangle = \frac{1}{N_{\mathbf{k}}} \begin{pmatrix} E(\mathbf{k}) + \mathcal{M}(\mathbf{k}) \\ ivk_x + Ak \end{pmatrix} \otimes \begin{pmatrix} \cos \frac{\theta_{\mathbf{k}}}{2} \\ \sin \frac{\theta_{\mathbf{k}}}{2} e^{i\phi_{\mathbf{k}}} \end{pmatrix}, \quad |\mathbf{k}, \beta'\rangle = \frac{1}{N_{\mathbf{k}}} \begin{pmatrix} E(\mathbf{k}) + \mathcal{M}(\mathbf{k}) \\ ivk_x - Ak \end{pmatrix} \otimes \begin{pmatrix} -\sin \frac{\theta_{\mathbf{k}}}{2} e^{-i\phi_{\mathbf{k}}} \\ \cos \frac{\theta_{\mathbf{k}}}{2} \end{pmatrix}, \quad (\text{S7})$$

where $E(\mathbf{k}) = \sqrt{\mathcal{M}^2(\mathbf{k}) + v^2k_x^2 + A^2k^2}$, the normalization factor $N_{\mathbf{k}} = \sqrt{(E(\mathbf{k}) + \mathcal{M}(\mathbf{k}))^2 + (v^2k_x^2 + A^2k^2)}$. We now construct the pseudospin basis $|\mathbf{k}, \alpha\rangle, |\mathbf{k}, \beta\rangle$ with $|\mathbf{k}, \alpha'\rangle, |\mathbf{k}, \beta'\rangle$. Following the general scheme in Ref. [S8–S11], we first find the representation of spin operators, and construct a new basis formed by linear combinations of $|\mathbf{k}, \alpha'\rangle, |\mathbf{k}, \beta'\rangle$ under which the spin- z -component operator σ_z is diagonal. Then, we choose a proper phase factor such that the new basis vectors transform formally as spins under symmetry operations. Explicitly, the matrix representations

of spin in $(|\mathbf{k}, \alpha'\rangle, |\mathbf{k}, \beta'\rangle)^T$ are given by

$$\langle \sigma_x \rangle = \begin{pmatrix} \sin \theta_{\mathbf{k}} \cos \phi_{\mathbf{k}} & W_{\mathbf{k}} e^{-i\phi_{\mathbf{k}}} (\cos \theta_{\mathbf{k}} \cos \phi_{\mathbf{k}} + i \sin \phi_{\mathbf{k}}) \\ W_{\mathbf{k}}^* e^{i\phi_{\mathbf{k}}} (\cos \theta_{\mathbf{k}} \cos \phi_{\mathbf{k}} - i \sin \phi_{\mathbf{k}}) & -\sin \theta_{\mathbf{k}} \cos \phi_{\mathbf{k}} \end{pmatrix}, \quad (\text{S8})$$

$$\langle \sigma_y \rangle = \begin{pmatrix} \sin \theta_{\mathbf{k}} \sin \phi_{\mathbf{k}} & -i W_{\mathbf{k}} e^{-i\phi_{\mathbf{k}}} (\cos \phi_{\mathbf{k}} + i \cos \theta_{\mathbf{k}} \sin \phi_{\mathbf{k}}) \\ i W_{\mathbf{k}}^* e^{i\phi_{\mathbf{k}}} (\cos \phi_{\mathbf{k}} - i \cos \theta_{\mathbf{k}} \sin \phi_{\mathbf{k}}) & -\sin \theta_{\mathbf{k}} \sin \phi_{\mathbf{k}} \end{pmatrix}, \quad (\text{S9})$$

$$\langle \sigma_z \rangle = \begin{pmatrix} \cos \theta_{\mathbf{k}} & -W_{\mathbf{k}} e^{-i\phi_{\mathbf{k}}} \sin \theta_{\mathbf{k}} \\ -W_{\mathbf{k}}^* e^{i\phi_{\mathbf{k}}} \sin \theta_{\mathbf{k}} & -\cos \theta_{\mathbf{k}} \end{pmatrix}, \quad (\text{S10})$$

where $W_{\mathbf{k}} = \frac{(E(\mathbf{k}) + \mathcal{M}(\mathbf{k}))^2 - (A\mathbf{k} - i v \mathbf{k}_x)^2}{N_{\mathbf{k}}^2}$. The positive eigenvalues of the above spin matrices are: $(\sqrt{\sin^2 \theta_{\mathbf{k}} \cos^2 \phi_{\mathbf{k}} + |W_{\mathbf{k}}|^2 (\cos^2 \theta_{\mathbf{k}} \cos^2 \phi_{\mathbf{k}} + \sin^2 \phi_{\mathbf{k}})}, \sqrt{\sin^2 \theta_{\mathbf{k}} \sin^2 \phi_{\mathbf{k}} + |W_{\mathbf{k}}|^2 (\cos^2 \theta_{\mathbf{k}} \sin^2 \phi_{\mathbf{k}} + \cos^2 \phi_{\mathbf{k}})}, \lambda_{\mathbf{k}})$, where $\lambda_{\mathbf{k}} = \sqrt{\cos^2 \theta_{\mathbf{k}} + |W_{\mathbf{k}}|^2 \sin^2 \theta_{\mathbf{k}}}$, $|W_{\mathbf{k}}|^2 = \sqrt{1 - A^2 k^2 / E^2(\mathbf{k})}$. By taking proper linear combinations of $|\mathbf{k}, \alpha'\rangle, |\mathbf{k}, \beta'\rangle$ [S8–S10], the pseudospin basis can be obtained as

$$|\mathbf{k}, \alpha\rangle = \frac{e^{-i\frac{\alpha_{\mathbf{k}}}{2}}}{\sqrt{|W_{\mathbf{k}}|^2 \sin^2 \theta_{\mathbf{k}} + (\cos \theta_{\mathbf{k}} - \lambda_{\mathbf{k}})^2}} (W_{\mathbf{k}} \sin \theta_{\mathbf{k}} |\mathbf{k}, \alpha'\rangle + (\cos \theta_{\mathbf{k}} - \lambda_{\mathbf{k}}) e^{i\phi_{\mathbf{k}}} |\mathbf{k}, \beta'\rangle) \quad (\text{S11})$$

$$|\mathbf{k}, \beta\rangle = \frac{e^{i\frac{\alpha_{\mathbf{k}}}{2}}}{\sqrt{|W_{\mathbf{k}}|^2 \sin^2 \theta_{\mathbf{k}} + (\cos \theta_{\mathbf{k}} - \lambda_{\mathbf{k}})^2}} ((\lambda_{\mathbf{k}} - \cos \theta_{\mathbf{k}}) e^{-i\phi_{\mathbf{k}}} |\mathbf{k}, \alpha'\rangle + W_{\mathbf{k}}^* \sin \theta_{\mathbf{k}} |\mathbf{k}, \beta'\rangle) \quad (\text{S12})$$

where $e^{i\alpha_{\mathbf{k}}} = \frac{W(\mathbf{k})}{|W(\mathbf{k})|}$. It is straightforward to see $T|\mathbf{k}, \alpha\rangle = |-\mathbf{k}, \beta\rangle$, $T|\mathbf{k}, \beta\rangle = -|-\mathbf{k}, \alpha\rangle$, $P|\mathbf{k}, \alpha\rangle = |-\mathbf{k}, \alpha\rangle$, $P|\mathbf{k}, \beta\rangle = |-\mathbf{k}, \beta\rangle$ (note that under time-reversal operation $\phi_{\mathbf{k}} \rightarrow \pi + \phi_{\mathbf{k}}$, $\theta_{\mathbf{k}} \rightarrow \pi - \theta_{\mathbf{k}}$, $\alpha_{\mathbf{k}} \rightarrow -\alpha_{\mathbf{k}}$). The representations of $\sigma_x, \sigma_y, \sigma_z$ in the pseudospin basis $\{|\mathbf{k}, \alpha\rangle, |\mathbf{k}, \beta\rangle\}$ are

$$\begin{aligned} \tilde{\sigma}_x(\mathbf{k}) &= \begin{pmatrix} \frac{1-|W_{\mathbf{k}}|^2}{2\lambda_{\mathbf{k}}} \sin(2\theta_{\mathbf{k}}) \cos \phi_{\mathbf{k}} & |W_{\mathbf{k}}| e^{-i\phi_{\mathbf{k}}} (\frac{\cos \phi_{\mathbf{k}}}{\lambda_{\mathbf{k}}} + i \sin \phi_{\mathbf{k}}) \\ |W_{\mathbf{k}}| e^{i\phi_{\mathbf{k}}} (\frac{\cos \phi_{\mathbf{k}}}{\lambda_{\mathbf{k}}} - i \sin \phi_{\mathbf{k}}) & \frac{|W_{\mathbf{k}}|^2 - 1}{2\lambda_{\mathbf{k}}} \sin(2\theta_{\mathbf{k}}) \cos \phi_{\mathbf{k}} \end{pmatrix} \\ &= |W_{\mathbf{k}}| (\frac{\cos^2 \phi_{\mathbf{k}}}{\lambda_{\mathbf{k}}} + \sin^2 \phi_{\mathbf{k}}) \rho_1 + |W_{\mathbf{k}}| \sin \phi_{\mathbf{k}} \cos \phi_{\mathbf{k}} (\frac{1}{\lambda_{\mathbf{k}}} - 1) \rho_2 + \frac{1 - |W_{\mathbf{k}}|^2}{2\lambda_{\mathbf{k}}} \sin(2\theta_{\mathbf{k}}) \cos \phi_{\mathbf{k}} \rho_3 \end{aligned} \quad (\text{S13})$$

$$\begin{aligned} \tilde{\sigma}_y(\mathbf{k}) &= \begin{pmatrix} \frac{1-|W_{\mathbf{k}}|^2}{2\lambda_{\mathbf{k}}} \sin(2\theta_{\mathbf{k}}) \sin \phi_{\mathbf{k}} & |W_{\mathbf{k}}| e^{-i\phi_{\mathbf{k}}} (\frac{\sin \phi_{\mathbf{k}}}{\lambda_{\mathbf{k}}} - i \cos \phi_{\mathbf{k}}) \\ |W_{\mathbf{k}}| e^{i\phi_{\mathbf{k}}} (\frac{\sin \phi_{\mathbf{k}}}{\lambda_{\mathbf{k}}} + i \cos \phi_{\mathbf{k}}) & \frac{|W_{\mathbf{k}}|^2 - 1}{2\lambda_{\mathbf{k}}} \sin(2\theta_{\mathbf{k}}) \sin \phi_{\mathbf{k}} \end{pmatrix} \\ &= |W_{\mathbf{k}}| \sin \phi_{\mathbf{k}} \cos \phi_{\mathbf{k}} (\frac{1}{\lambda_{\mathbf{k}}} - 1) \rho_1 + |W_{\mathbf{k}}| (\frac{\sin^2 \phi_{\mathbf{k}}}{\lambda_{\mathbf{k}}} + \cos^2 \phi_{\mathbf{k}}) \rho_2 + \frac{1 - |W_{\mathbf{k}}|^2}{2\lambda_{\mathbf{k}}} \sin(2\theta_{\mathbf{k}}) \sin \phi_{\mathbf{k}} \rho_3 \\ \tilde{\sigma}_z(\mathbf{k}) &= \lambda_{\mathbf{k}} \begin{pmatrix} 1 & 0 \\ 0 & -1 \end{pmatrix} = \lambda_{\mathbf{k}} \rho_3 \end{aligned} \quad (\text{S14})$$

For notational convenience, we define $\tilde{\sigma}_i(\mathbf{k}) = \sum_j a_{ij}(\mathbf{k}) \rho_j$. $a_{ij}(\mathbf{k})$ captures the effect of SOPC on the spin properties, ρ_j is the Pauli matrix defined in the pseudospin basis. It can be verified that under all symmetry operations, $\tilde{\sigma}_i(\mathbf{k})$ has the same transformation rules as spins. By projecting the full BdG Hamiltonian to the pseudospin basis, the pairing Hamiltonian is

$$H_s = \Delta \sum_{\mathbf{k}} c_{\mathbf{k}p,\uparrow}^\dagger c_{-\mathbf{k}p,\downarrow}^\dagger + c_{\mathbf{k}d,\uparrow}^\dagger c_{-\mathbf{k}d,\downarrow}^\dagger + h.c. \approx \Delta \sum_{\mathbf{k}} \psi_{\mathbf{k},\alpha}^\dagger \psi_{-\mathbf{k},\beta}^\dagger + h.c.. \quad (\text{S15})$$

Note that the form of s -wave pairing is preserved, *i.e.*, pseudospin-up and pseudospin-down states with opposite momentum are paired. This leads to the final form (as in Eq.3 of the main text) of the effective pairing Hamiltonian in the Nambu pseudospin basis $\Psi_{\mathbf{k}}^\dagger = (\psi_{\mathbf{k},\alpha}^\dagger, \psi_{\mathbf{k},\beta}^\dagger, \psi_{-\mathbf{k},\beta}, -\psi_{-\mathbf{k},\alpha})$:

$$H_{\text{eff}} = \sum_{\mathbf{k}, l, l'} \psi_{\mathbf{k}, l}^\dagger (\xi_+(\mathbf{k}) \delta_{l, l'} + \frac{1}{2} g_s u_B \mathbf{B} \cdot \tilde{\boldsymbol{\sigma}}_{l, l'}(\mathbf{k})) \psi_{\mathbf{k}, l'} + \Delta \sum_{\mathbf{k}} \psi_{\mathbf{k}, \alpha}^\dagger \psi_{-\mathbf{k}, \beta}^\dagger + h.c., \quad (\text{S16})$$

where l labels α, β , $\xi_{\pm}(\mathbf{k}) = \epsilon_0(\mathbf{k}) + E(\mathbf{k})$. In the following, we neglect the $+$ index, *i.e.*, $\xi_{\mathbf{k}} \equiv \xi_+(\mathbf{k})$.

PAULI SPIN SUSCEPTIBILITY AND RENORMALIZATION FACTOR γ_i

In general, the Pauli spin susceptibility with mean-field order parameter Δ is given by

$$\chi_s^{ij} = -\frac{1}{2}u_B^2 k_B T \sum_{\mathbf{k}} \sum_{\omega_n} \text{Tr}[\tilde{\sigma}_i \mathcal{G}^0(\mathbf{k}, i\omega_n) \tilde{\sigma}_j \mathcal{G}^0(\mathbf{k}, i\omega_n)]. \quad (\text{S17})$$

Here $\mathcal{G}^0(\mathbf{k}, i\omega_n) = (i\omega_n - \xi_{\mathbf{k}}\eta_3 - \Delta\eta_1)^{-1} = -\frac{i\omega_n + \xi_{\mathbf{k}}\eta_3 + \Delta\eta_1}{\omega_n^2 + \xi_{\mathbf{k}}^2 + \Delta^2}$ is the Nambu-Gor'kov Green's function. The factor 1/2 results from the particle-hole redundancy of Nambu basis. Eq.S17 is equivalent to the spin susceptibility formula given in Ref. [S12, S13]. By tracing out the pseudospin and particle-hole indices, we obtain

$$\chi_s^{ii} = -u_B^2 k_B T \sum_{\mathbf{k}} \sum_{\omega_n} \gamma_i(\mathbf{k}) \frac{-\omega_n^2 + \xi_{\mathbf{k}}^2 + \Delta^2}{(\omega_n^2 + \Delta^2 + \xi_{\mathbf{k}}^2)^2} \quad (\text{S18})$$

where $\gamma_i(\mathbf{k}) = 2 \sum_j a_{ij}^2(\mathbf{k})$ is the renormalization factor due to SOPCs, which are given explicitly by

$$\gamma_x(\mathbf{k}) = \frac{4|W_{\mathbf{k}}|^2 + (1 - |W_{\mathbf{k}}|^2)^2 \sin^2 2\theta_{\mathbf{k}}}{2(\cos^2 \theta_{\mathbf{k}} + |W_{\mathbf{k}}|^2 \sin^2 \theta_{\mathbf{k}})} \cos^2 \phi_{\mathbf{k}} + 2|W_{\mathbf{k}}|^2 \sin^2 \phi_{\mathbf{k}} \quad (\text{S19})$$

$$\gamma_y(\mathbf{k}) = \frac{4|W_{\mathbf{k}}|^2 + (1 - |W_{\mathbf{k}}|^2)^2 \sin^2 2\theta_{\mathbf{k}}}{2(\cos^2 \theta_{\mathbf{k}} + |W_{\mathbf{k}}|^2 \sin^2 \theta_{\mathbf{k}})} \sin^2 \phi_{\mathbf{k}} + 2|W_{\mathbf{k}}|^2 \cos^2 \phi_{\mathbf{k}} \quad (\text{S20})$$

$$\gamma_z(\mathbf{k}) = 2(\cos^2 \theta_{\mathbf{k}} + |W_{\mathbf{k}}|^2 \sin^2 \theta_{\mathbf{k}}). \quad (\text{S21})$$

By summing over the Matsubara frequencies in Eq.S18 first, the form of spin susceptibility can be further simplified to

$$\chi_s^{ii} = \frac{1}{2}u_B^2 \beta \sum_{\mathbf{k}} \gamma_i(\mathbf{k}) \frac{1}{1 + \cosh(\beta\sqrt{\xi_{\mathbf{k}}^2 + \Delta^2})}. \quad (\text{S22})$$

Note that at zero temperature, the residue spin susceptibility χ_s^{ii} vanishes since $\cosh(\beta\sqrt{\xi_{\mathbf{k}}^2 + \Delta^2}) \rightarrow \infty$. By taking $\Delta \rightarrow 0$, the normal-state spin susceptibility is recovered:

$$\chi_n^{ii} = \frac{1}{2}u_B^2 \beta \sum_{\mathbf{k}} \gamma_i(\mathbf{k}) \frac{1}{1 + \cosh(\beta\xi_{\mathbf{k}})} = u_B^2 N(E_F) \langle \gamma_i(E_F) \rangle. \quad (\text{S23})$$

Here $\langle \gamma_i(E_F) \rangle = \int d^2\mathbf{k} \gamma_i(\mathbf{k}) \delta(\xi_{\mathbf{k}} - E_F) / \int d^2\mathbf{k} \delta(\xi_{\mathbf{k}} - E_F)$ is the average value of γ_i over the Fermi surface. Obviously, in the zero temperature limit, the normal-state spin susceptibility is controlled by $\gamma_i(\mathbf{k})$, which can take a value within $[0, 2]$. To see how $\gamma_i(\mathbf{k})$ is affected by SOPCs, we note that if SOPC is absent, *i.e.*, $A\mathbf{k} = 0$, then $|W_{\mathbf{k}}| = 1$ and $\gamma_i = 2$. As we discussed in the main text, in this case the in-plane B_{c2} reduces to B_p . Upon increasing the SOPC strength, $|W_{\mathbf{k}}|$ is reduced, which reduces the value of $\gamma_i(\mathbf{k})$ and results in $B_{c2} > B_p$.

We note that there is another equivalent form of spin susceptibility obtained by performing the momentum integral first for Eq.S18:

$$\chi_s^{ii} / \chi_n^{ii} = 1 - \pi k_B T \sum_{\omega_n} \frac{\Delta^2}{(\Delta^2 + \omega_n^2)^{3/2}}, \quad (\text{S24})$$

where χ_n^{ii} is the reduced normal spin susceptibility. This form would provide a more straightforward way to understand disorder effects on the enhancement of B_{c2} as we shall discuss in details in Section VI.

B_{c2} FROM THE LINEARIZED GAP EQUATION

Here, we present details of the linearized gap equation we used to obtain the enhancement of B_{c2} shown in Fig.3 of the main text. Given the pairing Hamiltonian

$$H = \sum_{\mathbf{k}, l, l'} \psi_{\mathbf{k}, l}^\dagger (\xi_{\mathbf{k}} \delta_{l, l'} + u_B \mathbf{B} \cdot \tilde{\boldsymbol{\sigma}}) \psi_{\mathbf{k}, l'} - \frac{U}{2V} \sum_{\mathbf{k}} \psi_{\mathbf{k}, \alpha}^\dagger \psi_{-\mathbf{k}, \beta}^\dagger \psi_{-\mathbf{k}, \beta} \psi_{\mathbf{k}, \alpha}, \quad (\text{S25})$$

the corresponding linearized gap equation is given by

$$\frac{2}{U/V} = k_B T \sum_{\mathbf{k}} \sum_n \text{Tr}[G^{(0)}(\mathbf{k}, i\omega_n) \rho_y G^{(0)T}(-\mathbf{k}, -i\omega_n) \rho_y]. \quad (\text{S26})$$

Upon further simplifications and Matsubara sum, we have

$$\frac{1}{U/V} = k_B T \sum_{\mathbf{k}} \sum_n \frac{(i\omega_n - \xi_{\mathbf{k}})(-i\omega_n - \xi_{\mathbf{k}}) - u_B^2 \sum_j (\sum_i a_{ij}(\mathbf{k}) B_i)^2}{((i\omega_n - \xi_{\mathbf{k}})^2 - u_B^2 \sum_j (\sum_i a_{ij}(\mathbf{k}) B_i)^2)((-i\omega_n - \xi_{\mathbf{k}})^2 - u_B^2 \sum_j (\sum_i a_{ij}(\mathbf{k}) B_i)^2)}, \quad (\text{S27})$$

$$\frac{1}{U/V} = k_B T \sum_{\mathbf{k}} \frac{\sinh \beta \xi}{2\xi (\cosh \beta \xi + \cosh(\beta u_B B_{eff}(\mathbf{k})))}, \quad (\text{S28})$$

where $B_{eff} = \sqrt{\sum_i (a_{ij}(\mathbf{k}) B_i)^2}$. For magnetic field along the i -direction, $B_{eff} = B_i \sqrt{\gamma_k/2}$. In the absence of magnetic fields,

$$\frac{1}{U/V} = k_B T_c \sum_{\mathbf{k}} \frac{\sinh \beta \xi}{2\xi (\cosh \beta \xi + 1)} = k_B T_c N(E_F) \int_{-\hbar\omega_D}^{\hbar\omega_D} d\xi \frac{\tanh \beta \xi / 2}{2\xi} = N(E_F) \ln\left(\frac{2e^\gamma \hbar\omega_D}{\pi k_B T_c}\right), \quad (\text{S29})$$

Here, γ is the Euler constant, T_c is the zero field critical temperature. Substituting the expression of $\frac{1}{U/V}$ in Eq.S29 into Eq.S27, we get

$$\ln\left(\frac{T}{T_c}\right) = \int_{-\infty}^{+\infty} d\xi \int_0^{2\pi} \frac{d\varphi}{2\pi} \frac{\sinh \beta \xi}{2\xi} \left(\frac{1}{\cosh \beta \xi + \cosh(\beta u_B B_{eff}(E_F, \varphi))} - \frac{1}{\cosh \beta \xi + 1} \right) \quad (\text{S30})$$

Due to the complicated $a_{ij}(\mathbf{k})$ coefficients, the linearized gap equation was solved numerically by transforming the energy integral into a summation over momentum.

DERIVATION OF SUPERCONDUCTING FREE ENERGY

As we discussed in the main text, the scheme of linearized gap equation fails to capture the first-order phase transition at B_{c2} for the centrosymmetric spin-orbit-parity coupled(SOPC) superconductor WTe₂. As the in-plane field increases and approaches the superconductor-metal phase boundary, the superconducting gap and the value of B_{c2} need to be determined self-consistently by the minimum of the superconducting free energy f_s of the system. Here, we present a detailed derivation of the expression of f_s in the main text, which allows us to obtain the evolution of f_s under magnetic fields and the full superconducting phase diagram shown in Fig.4 of the main text.

In general, the partition function of a system involving two-body interactions can be written as:

$$Z = \int D[\psi(\mathbf{r}, \tau), \bar{\psi}(\mathbf{r}, \tau)] \exp\{-S[\psi(\mathbf{r}, \tau), \bar{\psi}(\mathbf{r}, \tau)]\}, \quad (\text{S31})$$

where the action is given by

$$S[\psi, \bar{\psi}] = \int d\tau \int d\mathbf{r} \sum_{\sigma} \bar{\psi}(\mathbf{r}, \tau) \partial_{\tau} \psi(\mathbf{r}, \tau) + \sum_{\sigma\sigma'} \bar{\psi}_{\sigma}(\mathbf{r}, \tau) H_0(\mathbf{r}, \tau) \psi_{\sigma'}(\mathbf{r}, \tau) - g \sum_{\sigma\sigma'} \bar{\psi}_{\sigma}(\mathbf{r}, \tau) \bar{\psi}_{\sigma'}(\mathbf{r}, \tau) \psi_{\sigma'}(\mathbf{r}, \tau) \psi_{\sigma}(\mathbf{r}, \tau). \quad (\text{S32})$$

By introducing an auxiliary bosonic field, the interaction term can be reformulated via the Hubbard-Stratonovich transformation:

$$\exp(g \int d\tau \int d\mathbf{r} \bar{\psi}_{\uparrow} \bar{\psi}_{\downarrow} \psi_{\downarrow} \psi_{\uparrow}) = \int D[\bar{\Delta}, \Delta] \exp(- \int d\tau \int d\mathbf{r} [\frac{1}{g} |\Delta|^2 - \Delta \bar{\psi}_{\uparrow} \bar{\psi}_{\downarrow} - \bar{\Delta} \psi_{\downarrow} \psi_{\uparrow}]), \quad (\text{S33})$$

Then, the action becomes

$$Z = \int D[\bar{\psi}(\mathbf{r}, \tau), \psi(\mathbf{r}, \tau)] \int D[\bar{\Delta}, \Delta] \exp(-S). \quad (\text{S34})$$

Here

$$S = \frac{1}{2} \int d\tau \int d\mathbf{r} \bar{\Phi} G^{-1} \Phi + \frac{1}{g} |\Delta|^2, \quad (\text{S35})$$

where $\Phi = (\bar{\psi}_\uparrow, \bar{\psi}_\downarrow, \psi_\uparrow, \psi_\downarrow)$ and

$$G^{-1} = \begin{pmatrix} \partial_\tau + H_0 & \Delta i\sigma_y \\ (\Delta i\sigma_y)^\dagger & \partial_\tau - H_0^* \end{pmatrix}. \quad (\text{S36})$$

Integrate out the Grassman field $\psi(\mathbf{r}, \tau)$, we have

$$Z = \int D[\bar{\Delta}, \Delta] \exp(-S_{eff}), \quad (\text{S37})$$

where $S_{eff} = \int d\tau \int d\mathbf{r} \frac{1}{g} |\Delta|^2 + \ln \text{Det} G^{-1}$. Within the mean-field approximation, Δ is assumed to be uniform in space and time. This reduces the mean-field free energy to the form

$$f_s = \frac{1}{\beta} \ln(Z) = \frac{1}{\beta} S_{eff} = \frac{V}{g} |\Delta|^2 - \frac{1}{\beta} \ln \text{Det} G^{-1} = \frac{V}{g} |\Delta|^2 - \frac{1}{\beta} \sum_{\mathbf{k}, n} \ln(1 + e^{-\beta \epsilon_{\mathbf{k}, n}}). \quad (\text{S38})$$

Here, V is the volume of system. The quasi-particle energies $\epsilon_{\mathbf{k}, n}$ are calculated from the full Bogoliubovde Gennes Hamiltonian $H_{BdG} = H_0(\mathbf{k})\eta_3 + \frac{1}{2}g_s u_B \mathbf{B} \cdot \boldsymbol{\sigma} + \Delta\eta_1$.

SPIN SUSCEPTIBILITY WITH NON-MAGNETIC IMPURITY SCATTERING

We discussed briefly in the main text that the enhancement of B_{c2} in SOPC superconductor is not affected in a qualitative way by disorder. Here we present detailed analysis of disorder effects on the SOPC superconductor WTe₂. Including both local potential fluctuation and spin-orbit scattering, the non-magnetic impurity potential can be written as [S14]

$$U_{im}(\mathbf{k} - \mathbf{k}') = U_1(\mathbf{k} - \mathbf{k}')\eta_3 + U_2(\mathbf{k} - \mathbf{k}')i(\hat{\mathbf{k}} \times \hat{\mathbf{k}}') \cdot \boldsymbol{\sigma}\eta_3 \quad (\text{S39})$$

$$= U_1(\mathbf{k} - \mathbf{k}')\eta_3 + U_2(\mathbf{k} - \mathbf{k}')i\lambda_{\mathbf{k}}\rho_3\eta_3(\hat{\mathbf{k}} \times \hat{\mathbf{k}}') \cdot \hat{z} \quad (\text{S40})$$

The diagrammatic calculation process to obtain the disorder-averaged spin suscepibility under $U_{im}(\mathbf{k} - \mathbf{k}')$ is shown in Fig.S2: following similar procedures in previous works [S13–S17], we first calculate the self-energy correction with the standard Born approximation. Then, we calculate the ladder diagram for the spin vertex correction, and finally obtain the disorder-averaged spin susceptibility as:

$$\overline{\chi_s^{ij}} = -\frac{1}{2}u_B^2 k_B T \sum_{\mathbf{k}} \sum_{\omega_n} \text{Tr}[\tilde{\sigma}_i \mathcal{G}(\mathbf{k}, i\omega_n) \Pi(\mathbf{k}, i\omega_n) \cdot \tilde{\sigma}_j \mathcal{G}(\mathbf{k}, i\omega_n)]. \quad (\text{S41})$$

Here $\mathcal{G}(\mathbf{k}, i\omega_n) = (i\omega_n - \xi_{\mathbf{k}}\eta_3 - \Delta\eta_1 - \Sigma(\mathbf{k}, i\omega_n))^{-1}$ is the Nam-Gor'kov Green's function including the self-energy correction due to disorder. The self-energy $\Sigma(\mathbf{k}, i\omega_n)$ is given by the self-consistent equation

$$\Sigma(\mathbf{k}, i\omega_n) = \int_{\mathbf{k}'} U_{im}(\mathbf{k} - \mathbf{k}') \mathcal{G}(\mathbf{k}', i\omega_n) U_{im}(\mathbf{k}' - \mathbf{k}), \quad (\text{S42})$$

where $\int_{\mathbf{k}} \equiv \int \frac{d^2\mathbf{k}}{(2\pi)^2}$. Within the Born approximation, the equation can be solved as

$$\Sigma(\mathbf{k}, i\omega_n) = -\frac{i\omega_n}{\tau\sqrt{\omega_n^2 + \Delta^2}} + \frac{\Delta}{\tau\sqrt{\omega_n^2 + \Delta^2}}\eta_1, \quad (\text{S43})$$

where $1/\tau = 1/\tau_0 + 1/\tau_{so}$ with

$$\frac{1}{\tau_0} = \pi N(E_F) \int d^2\mathbf{k}' \delta(\xi_{\mathbf{k}'} - E_F) |U_1(\mathbf{k} - \mathbf{k}')|^2, \quad (\text{S44})$$

$$\frac{1}{\tau_{so}} = \pi N(E_F) \int d^2\mathbf{k}' \delta(\xi_{\mathbf{k}'} - E_F) \lambda_{\mathbf{k}}^2 |U_2(\mathbf{k} - \mathbf{k}')|^2 \sin^2 \varphi_{\mathbf{k}'}. \quad (\text{S45})$$

Here, τ is the total scattering time, τ_0 is the momentum relaxation time, τ_{so} is the spin-orbit scattering time. Similar to previous works [S13, S15–S17], we consider the leading order s -wave scattering channel only, thus τ can be treated as \mathbf{k} -independent. Then $\mathcal{G}(\mathbf{k}, i\omega_n)$ can be rewritten as $\mathcal{G}(\mathbf{k}, i\omega_n) = (i\tilde{\omega}_n - \xi_{\mathbf{k}}\eta_3 - \tilde{\Delta}\eta_1)^{-1}$, where

$$\tilde{\omega}_n = \omega_n + \frac{\omega_n}{\tau\sqrt{\omega_n^2 + \Delta^2}}, \quad \tilde{\Delta} = \Delta + \frac{\Delta}{\tau\sqrt{\omega_n^2 + \Delta^2}}. \quad (\text{S46})$$

Now, we use $\mathcal{G}(\mathbf{k}, i\omega)$ to calculate the spin vertex corrections. The recursive integral equation for vertex correction, as depicted by the Feynman diagram Fig.S2d, is given by

$$\Pi(\mathbf{k}, i\omega_n) \cdot \tilde{\sigma}_j = \tilde{\sigma}_j + \int_{\mathbf{k}'} U_{im}(\mathbf{k} - \mathbf{k}') \mathcal{G}(\mathbf{k}', i\omega_n) \Pi(\mathbf{k}', i\omega_n) \cdot \tilde{\sigma}_j \mathcal{G}(\mathbf{k}', i\omega_n) U_{im}(\mathbf{k}' - \mathbf{k}) \quad (\text{S47})$$

Here, $\Pi(\mathbf{k}, i\omega) \cdot \tilde{\sigma}_j$ is the spin vertex function, which can be decomposed as

$$\Pi(\mathbf{k}, i\omega) \cdot \tilde{\sigma}_j \equiv \sum_m \Pi_m(\mathbf{k}, i\omega) \langle a_{jm}(E_F) \rangle \rho_m, \quad (\text{S48})$$

where $a_{im}(E_F) = \int d^2\mathbf{k} a_{im}(\mathbf{k}) \delta(\xi_{\mathbf{k}} - E_F)$ and $a_{jm}(\mathbf{k})$ is given in Sec. . A self-consistent ansatz of Π_m for the integral equation above has the form

$$\Pi_m = \lambda_m^0 + \lambda_m^1 \eta_1. \quad (\text{S49})$$

Substitute it into Eq.S47, we have

$$\lambda_m^0 = 1 + \frac{\tilde{\Delta}^2}{\tau_m(\tilde{\Delta}^2 + \tilde{\omega}^2)^{3/2}} \lambda_m^0 + \frac{i\tilde{\omega}\tilde{\Delta}}{\tau_m(\tilde{\Delta}^2 + \tilde{\omega}^2)^{3/2}} \lambda_m^1, \quad (\text{S50})$$

$$\lambda_m^1 = -\frac{i\tilde{\omega}\tilde{\Delta}}{\tau_m(\tilde{\Delta}^2 + \tilde{\omega}^2)^{3/2}} \lambda_m^0 + \frac{\tilde{\omega}^2}{\tau_m(\tilde{\Delta}^2 + \tilde{\omega}^2)^{3/2}} \lambda_m^1, \quad (\text{S51})$$

where $1/\tau_m = 1/\tau_0 - 1/\tau_{so}$ for $m = 1, 2$ and $1/\tau_m = 1/\tau_0 + 1/\tau_{so} = 1/\tau$ for $m = 3$. Then we obtain

$$\lambda_m^0 = \frac{\tilde{\omega}^2}{\tilde{\Delta}^2 + \tilde{\omega}^2} + \frac{\tilde{\Delta}^2 \tau_m}{(-\sqrt{\tilde{\Delta}^2 + \tilde{\omega}^2} + \tau_m(\tilde{\Delta}^2 + \tilde{\omega}^2))}, \quad \lambda_m^1 = \frac{-i\tilde{\omega}\tilde{\Delta}}{(\tilde{\Delta}^2 + \tilde{\omega}^2)(-1 + \tau_m\sqrt{\tilde{\Delta}^2 + \tilde{\omega}^2})}. \quad (\text{S52})$$

Simplify them with Eq.S46, we get

$$\lambda_m^0 = 1 + \frac{\Delta^2}{\Delta^2 + \omega^2} \frac{1}{\tau_m\sqrt{\Delta^2 + \omega^2} + (\tau_m/\tau - 1)}, \quad \lambda_m^1 = -\frac{i\Delta\omega}{\Delta^2 + \omega^2} \frac{1}{\tau_m\sqrt{\Delta^2 + \omega^2} + (\tau_m/\tau - 1)}. \quad (\text{S53})$$

Before proceeding to the final result, we discuss more about the vertex correction coefficients λ_m^0 and λ_m^1 here. When $\tau_{so} \rightarrow \infty$, namely, in the absence of spin-orbit scattering, we find $\lambda_m^0 = 1 + \frac{\Delta^2}{\tau_0(\Delta^2 + \omega^2)^{3/2}}$, $\lambda_m^1 = -i\frac{\Delta\omega}{\tau_0(\Delta^2 + \omega^2)^{3/2}}$. The vertex correction function in this case is $\Pi_m(i\omega) = (1 - \frac{\partial \Sigma(i\omega)}{\partial i\omega})$, which is exactly the Ward's identity. We have this identity here because without spin-orbit scattering, the vertex behaves as a scalar and spin is a conserve quantity.

After taking both the self-energy and vertex corrections, we can evaluate the disorder-averaged spin susceptibility $\overline{\chi_s^{ii}}$ from Eq.S41:

$$\overline{\chi_s^{ii}}/\chi_n^{ii} = 1 - \pi k_B T \sum_{\omega_n} \frac{\Delta^2}{(\omega_n^2 + \Delta^2)^{\frac{3}{2}}} I_{E_F}^i(\omega_n, \Delta, \tau_0, \tau_{so}), \quad (\text{S54})$$

where χ_n^{ii} is the reduced Pauli spin susceptibility and

$$I_{E_F}^i = \sum_m \frac{2 \langle a_{im}^2(E_F) \rangle}{\langle \gamma_i(E_F) \rangle} \frac{1 + \frac{1}{\tau_m\sqrt{\omega_n^2 + \Delta^2} + \tau_m/\tau - 1}}{1 + \frac{1}{\tau\sqrt{\omega_n^2 + \Delta^2}}}. \quad (\text{S55})$$

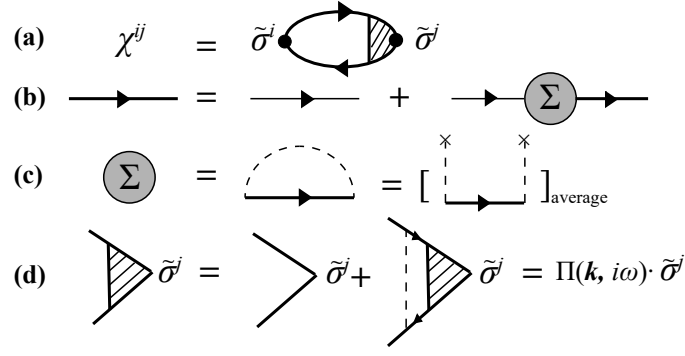


FIG. S2: Diagrammatic representation of (a) disorder-averaged spin susceptibility, (b) Dyson equation for self-energy correction, (c) self-energy in self-consistent Born approximation, (d) integral equation for spin vertex correction. The impurity potential is $U_{im}(\mathbf{k} - \mathbf{k}') = U_1(\mathbf{k} - \mathbf{k}') + U_2(\mathbf{k} - \mathbf{k}')i(\hat{\mathbf{k}} \times \hat{\mathbf{k}}') \cdot \boldsymbol{\sigma}$ [S16]. The first term describes scattering from scalar potential fluctuations, and the second term describes the spin-orbit scattering.

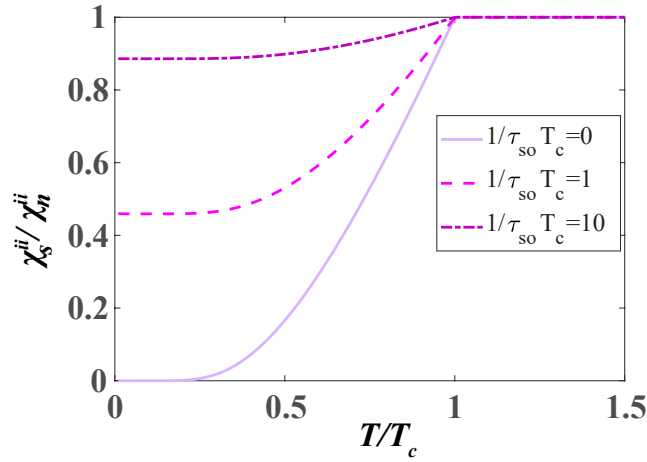


FIG. S3: Plot of χ_s^{ii}/χ_n^{ii} versus T/T_c in Eq.S57 for $i = x, y$. The strength of spin-orbit scattering is characterized by the dimensionless parameter $1/\tau_{so}T_c$. Evidently, the appearance of spin-orbit coupling generates finite residue spin susceptibility that can enhance the upper critical field.

Comparing with χ_s^{ii} in the clean case, we have an extra factor I_{EF}^i here that encodes the information of impurity scattering. When the spin-orbit scattering is absent, namely in the limit $\tau_{so} \rightarrow \infty$, we have $\tau_m = \tau_0 = \tau$, thus $I_{EF}^i = 1$ and we have

$$\overline{\chi_s^{ii}}/\chi_n^{ii} = 1 - \pi k_B T \sum_{\omega_n} \frac{\Delta^2}{(\Delta^2 + \omega_n^2)^{3/2}} = \chi_s^{ii}/\chi_n^{ii}. \quad (\text{S56})$$

Thus, without spin-orbit scattering, $\overline{\chi_s} = \chi_s$ as shown in Eq.S24 and the disorder-averaged spin susceptibility is unchanged. This can be seen directly from the ladder diagram: when the scalar Ward's identity is preserved, the self-energy correction cancels the vertex correction. This shows that the B_{c2} in SOPC superconductors is insensitive to the potential fluctuations induced by impurities.

With finite spin-orbit scattering, namely $\tau_{so}^{-1} \neq 0$,

$$I_{EF}^i(\omega_n, \Delta, \tau_0, \tau_{so}) = \frac{2 \langle a_{i3}(E_F) \rangle}{\langle \gamma_i(E_F) \rangle} + \sum_{m=1}^2 \frac{2 \langle a_{im}(E_F) \rangle}{\langle \gamma_i(E_F) \rangle} \frac{1 - \frac{1}{\tau_{so} \sqrt{\omega_n^2 + \Delta^2} + 2}}{1 + \frac{1}{\tau_{so} \sqrt{\omega_n^2 + \Delta^2}}}. \quad (\text{S57})$$

The coefficients $\langle a_{im}(E_F) \rangle$ and $\langle \gamma_i(E_F) \rangle$ capture the effect of SOPC on spin-orbit scattering. Plots of residue χ_s^{ii} ($i = x, y$) at different spin-orbit scattering strengths are shown in Fig.S3. Clearly, the presence of sufficiently strong spin-orbit scattering with $1/\tau_{so} \sim T_c \sim 0.1$ meV can give rise to a residue spin susceptibility to enhance the B_{c2} . However,

as the correction in χ_s does not affect the order of $\chi_n - \chi_s$, the enhancement of B_{c2} is not affected in a qualitative way given $B_{c2} = B_p \sqrt{\chi_0/(\chi_n - \chi_s)}$ as we discussed in the main text.

In conclusion, we find that B_{c2} in the SOPC superconductor is robust against scalar potential fluctuations and spin-orbit scattering may further enhance B_{c2} by inducing a residue χ_s .

* Corresponding author.

phlaw@ust.hk

- [S1] X. Qian, J. Liu, L. Fu, and J. Li, *Science* **346**, 1314 (2014).
- [S2] S. Tang et al., *Nature Physics* **13**, 683 (2017).
- [S3] L. Muechler, A. Alexandradinata, T. Neupert, and R. Car, *Phys. Rev. X* **6**, 041069 (2016).
- [S4] X. Lin and J. Ni, *Phys. Rev. B* **95**, 245436 (2017).
- [S5] D.-H. Choe, H.-J. Sung, and K. J. Chang, *Phys. Rev. B* **93**, 125109 (2016).
- [S6] L.-k. Shi and J. C. W. Song, *Phys. Rev. B* **99**, 035403 (2019).
- [S7] C.-X. Liu, X.-L. Qi, H. Zhang, X. Dai, Z. Fang, and S.-C. Zhang, *Phys. Rev. B* **82**, 045122 (2010).
- [S8] J. W. F. Venderbos, V. Kozii, and L. Fu, *Phys. Rev. B* **94**, 180504 (2016).
- [S9] L. Fu, *Phys. Rev. Lett.* **115**, 026401 (2015).
- [S10] S.-K. Yip, *Phys. Rev. B* **87**, 104505 (2013).
- [S11] S.-K. Yip, arXiv:1609.04152 (2016).
- [S12] P. A. Frigeri, D. F. Agterberg and M. Sigrist, *New Journal of Physics* **6**, 115 (2004).
- [S13] A. Abrikosov and L. Gor'kov, *Sov. Phys. JETP* **15**, 752 (1962).
- [S14] R. A. Klemm, A. Luther, and M. R. Beasley, *Phys. Rev. B* **12**, 877 (1975).
- [S15] B. Dóra, A. Virosztek, and K. Maki, *Phys. Rev. B* **66**, 115112 (2002).
- [S16] A. V. Balatsky, I. Vekhter, and J.-X. Zhu, *Rev. Mod. Phys.* **78**, 373 (2006).
- [S17] A. Abrikosov and L. Gorkov, *Sov. Phys. JETP* **8**, 1090 (1959).